HHS Public Access

Author manuscript

Mol Cancer Ther. Author manuscript; available in PMC 2018 April 01.

Published in final edited form as:

Mol Cancer Ther. 2017 April ; 16(4): 763–772. doi:10.1158/1535-7163.MCT-16-0644.

Targeted treatment of metastatic breast cancer by PLK1 siRNA delivered by an antioxidant nanoparticle platform

Jingga Morry[1,*], **Worapol Ngamcherdtrakul**[1,2,*], **Shenda Gu**[1], **Moataz Reda**[1], **David J. Castro**[1,2], **Thanapon Sangvanich**[1], **Joe W. Gray**[1,#], and **Wassana Yantasee**[1,2,#]

[1]Department of Biomedical Engineering, Oregon Health and Science University, 3303 SW Bond Ave, Portland, OR 97239, USA

[2]PDX Pharmaceuticals, LLC, 3303 SW Bond Ave, Portland, OR 97239, USA

Abstract

Metastatic breast cancer is developed in about 20–30% of newly diagnosed early stage breast cancer patients despite treatments. Herein, we report a novel nanoparticle platform with intrinsic anti-metastatic properties for the targeted delivery of Polo-like kinase 1 siRNA (siPLK1). We first evaluated it in a triple negative breast cancer (TNBC) model, which shows high metastatic potential. PLK1 was identified as the top therapeutic target for TNBC cells and tumor initiating cells in a kinome-wide screen. The platform consists of a 50-nm mesoporous silica nanoparticle (MSNP) core coated layer-by-layer with bioreducible cross-linked PEI and PEG polymers, conjugated with an antibody for selective uptake into cancer cells. SiRNA is loaded last and fully protected under the PEG layer from blood enzymatic degradation. The material has net neutral charge and low non-specific cytotoxicity. We have also shown for the first time that the MSNP itself inhibited cancer migration and invasion in TNBC cells owing to its ROS and NOX4 modulating properties. In vivo, siPLK1-nanoconstructs (6 doses of 0.5 mg/kg) knocked down about 80% of human PLK1 mRNA expression in metastatic breast cancer cells residing in mouse lungs, and reduced tumor incidence and burden in lungs and other organs of an experimental metastasis mouse model. Long-term treatment significantly delayed the onset of death in mice and improved the overall survival. The platform capable of simultaneously inhibiting the proliferative and metastatic hallmarks of cancer progression is unique and has great therapeutic potential to also target other metastatic cancers beyond TNBC.

Keywords

siRNA; metastasis; antioxidant; mesoporous silica; PLK1

[#]Corresponding authors. **Corresponding author contacts:** Joe W. Gray, 2730 SW Moody Ave, CL3G, Portland, OR 97201, Tel: 503-494-6500 | Fax: 503-418-9311 | grayjo@ohsu.edu, Wassana Yantasee, 3303 SW Bond Ave, CH13B, Portland, OR 97239, Tel: 503-418-9306 | Fax: 503-418-9311 | yantasee@ohsu.edu.

[*]Authors with equal contribution

The authors declare the following competing financial interest(s): OHSU, J.M., W.N., D.J.C., J.W.G., and W.Y. have a significant financial interest in PDX Pharmaceuticals, LLC, a company that may have a commercial interest in the results of this research and technology.

This potential personal and institutional conflict of interest has been reviewed and managed by OHSU.

Introduction

About 1.7 million new cases of breast cancer were diagnosed worldwide in 2012 (1) and around 250,000 more are expected to be diagnosed in the US in 2016 (2). About 20–30% of newly diagnosed early stage breast cancer patients will develop distant metastasis despite the treatments. There is no effective treatment for metastatic cancer so far, current treatment focuses on slowing disease progression and maintaining the quality of life. Targeted delivery of siRNAs by nanoparticles holds great promise for cancer treatment since siRNA can target any gene deemed important to cancer progression, metastasis, and drug resistance with high specificity (3). To that end, we have recently developed and optimized a polymer-coated mesoporous silica nanoparticles (NP) for siRNA delivery to treat trastuzumab-resistant HER2+ breast tumors (4). The platform consists of a 50-nm mesoporous silica nanoparticle (MSNP) core coated layer-by-layer with bioreducible cross-linked 10-kDa polyethyleneimine (PEI) for effective siRNA binding and endosomal escape, and polyethylene glycol (PEG) for preventing nanoparticle aggregation, minimizing enzyme degradation of siRNAs, shielding the toxic effect of PEI, and reducing recognition by the immune system. In addition, a targeting antibody can be attached to the PEG layer to serve as a homing agent on the nanoparticle. The siRNA is then loaded last onto the nanoparticle, passing the PEG layer (due to small size) and binding to the PEI layer due to charge preference (See Supplementary Fig. S1).

Herein, we report for the first time that the same platform can act as a targeted siRNA delivery system to metastatic breast tumors. For the siRNA target, we chose polo-like kinase 1 (PLK1), which is involved in cell division and DNA damage response and is found in actively dividing cancer cells (5). PLK1 was identified as a promising therapeutic target for cancer treatment (6). There is strong association between elevated PLK1 levels in breast tumors and poor clinical outcome (7). Moreover, a recent genome-wide kinase screen also identified PLK1 as the strongest kinase target as demonstrated by significant cell death in both cancer and tumor-initiating cells (TICs) in TNBC when either knocked down or inhibited (8). PLK1 inhibitor, BI2536, had reached clinical trials but was terminated due to poor therapeutic index since the systemic delivery of PLK1 inhibitors was associated with increased incidence neutropenia and thrombocytopenia (9). In addition, PLK1 inhibitors (e.g., BI2536, BI6727, GSK461364) can also inhibit other PLK family members PLK2 and PLK3, which may lead to unwanted off-target effects (10). In contrast, siRNA can be designed to target only PLK1, and thus have less toxicity to non-cancer cells than BI2536 (11). An siRNA against PLK1 (TKM-080301) has been in phase I/II trials by Arbutus Biopharma, but the delivery platform has no targeting agent and is lipid-based that is homing for liver. When used to treat liver tumors, stable disease in 51% of 43 patients was reported (12), but with a narrow therapeutic window due to toxicity (0.6–0.75 mg/kg) (13). We hypothesize that siRNA sequence specificity and the delivery specificity will improve both efficacy and safety.

Another unique and important feature about our platform is the inherent antioxidant activity of the mesoporous silica core. This antioxidant capability is shown herein to have pronounced effects in inhibiting EMT and cellular invasion *in vitro*. ROS plays an important role in cancer metastasis (14). ROS-generating NOX4 is crucial in redox-mediated signaling

pathways, including Tks5-dependent invadopodia formation (15), TGF-β/SMAD3-driven EMT and cell migration (16), and PI3K/Akt-regulated cell proliferation and invasion (17). Reduction of ROS using an antioxidant such as N-acetylcysteine (NAC) or the NOX inhibitor, Diphenyleneiodonium (DPI), successfully decreased cancer invasion and invadopodia formation (15). Nevertheless, these agents are not used in clinics for such purposes due to the inability to achieve sufficient cellular NAC levels based on the current prescribed dose (18) and the challenge of getting specificity to particular NOX isoforms (19). Thus, a material that can scavenge ROS at cellular levels can offer an effective therapy for metastatic breast cancer. Out of the 162 investigational new drugs (IND) in clinical trials for treating metastatic breast cancer, only one targets the cancers' ability to activate invasion and metastasis (a TGF-β inhibitor), and most target cancers' sustaining proliferative signaling (20). Our material is uniquely targeting both cancer hallmarks, making it highly novel.

Materials and Methods

Synthesis and characterization of nanoparticles and siRNA loading

Mesoporous silica nanoparticles (MSNPs) of 50 nm in size were synthesized and surface-modified as in our previous report (4). MSNP cores were measured for primary (dry) size by a Transmission Electron Microscope (Philips/FEI Tecnai TEM, Hillsboro, OR). After chemical modifications, the material was measured for hydrodynamic size in PBS (pH 7.2) with a Zetasizer (Malvern, Westborough, MA). PEI and PEG loadings were quantified by a thermogravimetric analyzer (TGA Q50, TA Instruments, New Castle, DE). siRNA loading was accomplished with 10 min mixing in PBS. The siRNA loading was quantified by fluorescence detection of dye-tagged siRNA as well as gel electrophoresis. The material contained 14 wt% 10-kDa PEI, 18 wt% 5-kDa PEG, 3 wt% antibody or no antibody, and 2 wt% siRNA. It is referred to as T-siRNA-NP with Trastuzumab (T) antibody, or siRNA-NP without (4). The particle size in PBS was 104 ± 1.7 nm, and the charge decreased from 13.3 ± 0.70 mV to 8.10 ± 0.25 mV once loaded with siRNA (measured in 10 mM NaCl), which falls within neutral range as defined by Nanotechnology Characterization Lab of NCI (21)). Schematic illustration of the nanoconstruct can be found in supplementary Fig. S1.

Cell culture and transfection

Human breast carcinoma cell lines, BT549 and MDA-MB-231, were obtained from American Type Cell Collection (ATCC) and maintained in RPMI with 10% FBS. LM2-4luc +/H2N (22), was a gift from Prof. Robert Kerbel (University of Toronto) and Prof. Giulio Francia (now at University of Texas at El Paso) and maintained in RPMI + 5% FBS. BT549 and MDA-MB-231 were authenticated by genotyping at the Sequencing Core of OHSU, and both matched genotypes available from ATCC. LM2-4luc+/H2N, a derived cell line as described in ref (22), was used as received and not authenticated in our lab. For NP transfection (loaded with siSCR or siPLK1), cells (3,000 cells/well in 96-well plates or 200,000 cells in 6 well plates) were seeded overnight in complete medium and transfected with NP for 24 h. The cells were washed once with PBS on the next day and incubated in a fresh cell media for 24 – 72 h post-treatment depending on the type of the assays. Positive controls were carried out using DharmaFECT-1 transfection reagent (GE Dharmacon,

Lafayettte, CO) diluted in OptiMEM medium (ThermoFisher Scientific, Eugene, OR). Unless stated otherwise, all experiments were performed with nanoparticle-to-siRNA mass ratio of 50 and 50 nM siRNA throughout the study.

siRNAs

Four different PLK1 siRNA sequences were purchased from Qiagen (cat. #1027416) for siRNA screening in the LM2-4luc+/H2N cell line. The *in vivo* grade siRNA was custom made by GE Dharmacon based on the sequence identified to yield the highest PLK1 gene knockdown and cell death in LM2-4luc+/H2N cells (see Supplementary Fig. S2). The siRNA sequences were as follows: optimal PLK1 (antisense 5-'UAUUCAUUCUUCUUGAUCCGG-3'); scrambled SCR (antisense 5'-UUAGUCGACAUGUAAACCA-3'). DY677-siSCR was custom made with DyLight 677 attached to the sense strand of the siSCR (GE Dharmacon).

Animal studies

The experimental protocol was approved by the Institutional Animal Care and Use Committee (IACUC) of Oregon Health and Science University (OHSU). 6–8 week old SCID hairless SHO™ (Crl:SHO-Prkdc^{scid}Hr^{hr}, Charles River, Wilmington, MA) mice received intravenous tail vein injections of 2×10^6 LM2-4luc+/H2N cells (suspended in 200 μL PBS) and were allowed to establish metastasis in lungs for 2 weeks before initiating the treatments. For both studies (short-term and long-term), all mice were randomly divided into three treatment groups (n = 8/group): Saline control, T-siSCR-NP (0.5 mg/kg siSCR), and T-siPLK1-NP (0.5 mg/kg siPLK1), with a dosing schedule of twice weekly by intravenous injection (Fig. 4A). IVIS imaging was done once weekly starting from 1 week post-inoculation, following the protocol established by Caliper Life Sciences, MA. Briefly, each animal received intraperitoneal injection of 150 mg/kg of D-luciferin (Gold Bio Technology, Inc, St. Louis, MO) in 200 μL PBS, 10 minutes prior to imaging with IVIS spectrum Imaging system on prone and supine positions. The average photon flux (of prone and supine positions) for each mouse was quantified within the same area of interest in the thoracic region of each mouse. The flux was plotted as average fold-change (relative to the pre-treatment signals of each mouse) as a function of time. Body weight was measured twice weekly. For the short-term *in vivo* study, all animals were sacrificed 2 days after receiving the 6th dose of treatment and their major organs (brain, heart, lung, liver, spleen, kidney, lymph nodes, and spine) were harvested and immersed in 300 μg/mL of D-luciferin (in PBS) in a 24-well plate for 5 minutes prior to *ex vivo* IVIS imaging and signal quantification. Organs with detectable IVIS signals compared to negative controls (i.e., the same organs from mice without tumor inoculation) were considered positive for the presence of cancer and included in 'incidence rate'. The tumor burden was calculated as the sum of all signals from each respective tumor-bearing organ.

For the long-term *in vivo* study, animals (8 animals per group) received the same dose and treatment schedule as the short term study but the study was extended to 2 months. Mice were monitored daily for signs of illness (hind limb paralysis from suspected spine metastasis, excessive weight loss (>10% body weight loss compared to the pre-inoculation weight), visible tumors (from lymph nodes, with size greater than 1500 mm^3), or labored

breathing from lung metastasis and were euthanized in accordance with IACUC ethical guidelines. All major organs were collected, weighed, and fixed for histological analyses.

Lung metastasis quantification

The lung tissues from each mouse were collected and fixed in 4% PFA and snap-frozen in OCT compound (#4583, Tissue-Tek) prior to processing. Tissue sections (6-μm thick) were stained with hematoxylin and eosin (H&E). To assess the metastatic area, 10 sections of the entire lung at 160 μm apart were scanned using ScanScope XT Digital Slide Scanner (Aperio), and the area of each metastatic lesion was measured relative to the total lung area.

For determination of the tumor burden and human PLK1 mRNA expression in mouse lungs, lung tissue from each mouse was homogenized and lysed in RLT buffer using QIA-shredder columns (Qiagen), and the RNA was isolated using RNeasy Mini kit (Qiagen) following the manufacturer's protocol. RT-PCR (100 ng RNA/sample per reaction) was performed to identify the ratio of human HPRT mRNA (Hs99999909_m1) relative to mouse HPRT mRNA (Mm03024075_m1) for tumor burden or human PLK1 mRNA (Hs00983225_g1) relative to human HPRT mRNA to assess PLK1 gene knockdown as a result of the treatments.

Statistical Analysis

In vitro experiments were performed in triplicates (experimentally and analytically), and results were presented as mean ± SD. *In vivo* experimental data were presented as mean ± SEM. Comparisons of all groups at a single time point were performed after testing for D'Agostino-Pearson omnibus normality tests (Graphpad Prism 6.0). Comparisons of two groups were performed either with Student's *t* tests (for normal distribution) or Mann-Whitney test (for nonparametric test, unpaired groups). For comparisons of more than three groups, statistical analysis was done either with one-way ANOVA with post-hoc Dunnett's multiple comparison tests (for normal distribution) or Kruskal-Wallis non-parametric test with post-hoc Dunnett's multiple comparison tests (for non-normal distribution). Two-way ANOVA followed by post-hoc Tukey's multiple comparison tests was performed to analyze the treatment effects over time in the photon flux measurement of the *in vivo* study. Survival curves were analyzed using Kaplan-Meier and its multiple comparison tests were analyzed using log-rank test methods with adjusted alpha by Bonferroni correction. Graphpad Prism 6.0 software (GraphPad software Inc., San Diego, CA) was utilized for all statistical analyses. P-value of < 0.05 was considered to be statistically significant.

Detailed procedures of intracellular ROS assay, cell viability assay, in vitro scratch assay, gelatin degradation, matrigel invasion assay, 3D culture, qPCR, western blot and histology can be found in the Supplementary Methods.

Results

PLK1 knockdown efficacy and resultant apoptotic cell death

We chose TNBC cell lines for the in vitro studies due to their high metastatic potential. To investigate the silencing efficacy of siPLK1-NP *in vitro*, we treated BT549, MDA-MB-231,

and LM2-4luc+/H2N (HER2-expressing MDA-MB-231 metastatic variant (22)) cell lines with siPLK1-NP (without targeting agent) and measured the mRNA and protein expressions 24 and 48 h post-treatment, respectively. As shown in Fig. 1A–B, siPLK1-NP efficiently reduced the PLK1 mRNA by 69–87% and protein expressions by 64–91% in the three cell lines compared to the untreated control. Consequently, the siPLK1-NP treatment induced significant loss of cell viability measured at 3 days (Fig. 1C). We also confirmed that the siPLK1-NP treatment caused G2/M cell cycle arrest at 24 h post treatment similar to the PLK1 inhibitor BI 2536 (Fig. 1D). On the contrary, non-targeting siSCR-NP did not cause any significant reduction in the PLK1 expression (Fig. 1A–B), was not toxic to the cells (~80% cell viability, Fig. 1C), and did not alter cell cycle arrest compared to the untreat (Fig. 1D). These results demonstrate that the NP is well tolerated, and can effectively deliver siPLK1 intracellularly, leading to apoptotic death of the TNBC cell lines.

Antioxidant and NOX4 reduction properties of NP in TNBC cell lines

From our recent report (23), the MSNP core of our NP had ROS scavenging and NOX4 reduction ability in TGF-β stimulated dermal fibroblast cells, yielding greater anti-fibrotic properties (e.g., reducing COL I and α-SMA) than observed with NAC treatment. Herein, we investigated the antioxidant effects of NP treatment on breast cancer cells. We included siSCR on the NP treatment in order to maintain similar size and charge of the nanoconstruct (and hence cellular uptake) as those of the siPLK1-NP. This siSCR does not have any significant sequence homology to known human or mouse genes. The ROS levels of all three TNBC cell lines were significantly higher (by 2–8 fold) than the non-tumorigenic breast epithelial cells line, MCF10A (Supplementary Figs. S3A–B). Pre-treatment of the breast cancer cell lines with siSCR-NP prior to ROS stimulation by menadione lowered the ROS levels by 60–84% compared to the menadione alone (Fig. 2A). The NP performed in a similar manner as the antioxidant NAC, and NADPH oxidase (NOX) inhibitor DPI. Since NOX is a major source of ROS production, we measured the mRNA levels of NOX family members in the TNBC cell lines *vs.* those in the non-tumorigenic breast epithelial cell line, MCF10A. Out of the four NOX family members tested, NOX4 mRNA levels were significantly higher (than NOX1, NOX3, and NOX5) for all the TNBC cell lines compared to MCF10A (Supplementary Fig. S3C). In addition to its high level, NOX4 (and ROS) has been shown to play very important roles in cancer invasion and metastasis via invadopodia formation (15), thus we further focused on NOX4. Treatment of siSCR-NP for 24 h was able to significantly reduce NOX4 mRNA in the TNBC cell lines by 37–56% compared to the untreated cells (Fig. 2B), similar to NAC and DPI. Interestingly, in terms of NOX4 protein reduction, siSCR-NP lowered NOX4 expression better than NAC and DPI after 72 h treatment (Fig. 2C), suggesting that NP may have more sustainable effect than NAC and DPI. Taken together, these results proved that NP, indeed, possessed ROS-scavenging ability. The NP's ability to reduce NOX4 expression upon ROS scavenging also indicates a positive feedback loop between ROS and NOX4. Interestingly, the nanoparticle did not significantly reduce the ROS level of the MCF10A (Supplementary Fig. S3D) likely due to the low baseline level of ROS and NOX4 in this cell line compared to the three TNBC cell lines (Supplementary Fig. S3A–C).

NP treatment inhibits cellular migration and invasion, and attenuates outgrowth of 3D-organotypic cultures

Elevated levels of ROS have been known to promote cellular migration as well as invasion (24). To investigate the effects of NP treatment on cellular migration, we performed an in vitro scratch assay using the LM2-4luc+/H2N cell line. We used NP without trastuzumab (T) throughout the migration, invasion, and 3D growth studies to ensure that any observed effect was due to the nanoparticle itself and not trastuzumab. The cells were wounded (25) following a 24 h pre-treatment with siSCR- or siPLK1-NP. DharmaFECT commercial transfection reagent delivering both siRNAs was also used as controls. We monitored wound closure at 24 h and reported it as the percent wound recovery relative to the wound size at t = 0 h. Fig. 3A shows the representative wound recovery images, and Fig. 3B shows the quantification. Cells treated with siSCR-NP and siPLK1-NP displayed the least wound recovery indicating slowest cell migration compared to the untreated control and DharmaFECT counterparts. This was not due to the siSCR or siPLK1, since when delivered with DharmaFECT, they showed no inhibitory effect on cell migration. Moreover, we delivered NP loaded with fluorescently labelled siRNA, DyLight 677 (DY677siSCR-NP) to ensure the effect was attributed to the intracellular presence of NP and not a physical hindrance at the wound border (Fig. 3A).

Next, we investigated the ability of NP to migrate through the extracellular matrix (ECM) by forming the actin-rich protrusions known as invadopodia. Specifically, we cultured cells that were pre-treated with siSCR-NP or DPI on thin fluorescent gel matrices for 24 h and measured the area of gelatin degradation. Higher gelatin degradation indicates higher invadopodia formation which correlates to the cellular invasive potential. As shown in Figs. 3C–D, siSCR-NP treatment reduced gelatin degradation activity by ~42% compared to the untreated groups, indicating reduction of invadopodia formation by the NP. The effect is on par with DPI treatment (~46%). To confirm our finding, we also measured the invasive capacity of the cells in a Matrigel-coated Boyden chamber assay. NP treatment markedly reduced the invasiveness of the cells by ~65%, in a similar manner as DPI (~60%), as compared to the untreated control (Fig. 3E). Only the high dose of NAC (30 mM) produced inhibitory effects on the invasiveness of the cells in the same par with NP and DPI. This is in agreement with previous report demonstrating that only a high NAC dose (20–40 mM) was able to reduce cancer cell invasion (15). Conversely, the observed increase in invaded cells at the low dose of NAC (2–5 mM, Fig. 3E) is also in line with another observation (26) showing that low levels of NAC increased cancer metastasis potential *in vivo*. However, high levels of NAC is not achievable in blood (not even 10 mM), based on the current prescribed dose of NAC (18). Thus, our antioxidant nanoparticle has a clear advantage over NAC. Specifically, much less dose of NP required to achieve the same effect as NAC may be attributed to extremely large scavenging sites (from large surface area of the MSNP, ~500 m^2/g).

To study the effects of NP treatment in a 3D environment, we seeded cells (pre-treated with DY677siSCR-NP) on matrigel-coated plates and observed the cell phenotypes from day 1 to day 5 post-seeding. LM2-4luc+/H2N cells grown in 3D culture exhibited stellate structures (Fig. 3F), which is typical for highly invasive cells such as its parental MDA-MB-231 cell

line (27). However, treatment with siSCR-NP inhibited the invasive growth patterns of these cells, resulting in more rounded spheroid structures. To ensure that NP was still present within the cells, we also imaged the cells in the fluorescence channel (for viewing DY677siSCR-NP) up to 5 days post seeding on matrigel (Fig. 3F). These experiments demonstrate that NP treatment effectively reduced cellular migration and invasiveness of a highly invasive breast cancer cell line *in vitro*.

Ability of T-NP to deliver siRNAs and elicit therapeutic effects in a mouse model of metastasis

A breast cancer metastasis model was established upon tail vein injection of LM2-4luc +/H2N cells (from Dr. Robert Kerbel lab. University of Toronto), a highly metastatic variant of MDA-MB-231 (TNBC) which were isolated from lung metastasis in mice (28) and has been shown to develop metastasis in multiple organs (29). This cell line was later engineered to express luciferase and HER2 genes (22). We found siPLK1 to be highly effective in killing this cell line (see Fig. 1). Despite overexpressing HER2, we found that this cell line behaved like its parental MDA-MB-231 cell in that it did not respond to trastuzumab (0–30 μg/ml) as a free drug or when conjugated to the NP (T-NP) *in vitro* (Supplementary Fig. S4). Nevertheless, the HER2 protein can serve as the homing target receptor to facilitate targeted delivery of siPLK1 utilizing the nanoparticle conjugated with trastuzumab (T-NP). The cellular uptake specificity of T-NP to HER2+ cells over HER2- cells has been previously reported (4). In mice, tumors were allowed to establish for 2 weeks until luciferase signals were detected in lungs by IVIS (Fig. 4B), followed by twice-weekly tail vein injections of T-siPLK1-NP for both the short- and long-term studies. Dosing and schedule are shown in Fig. 4A (frequency optimization as described in Supplementary Method). After a total of 6 doses treatment (0.5 mg/kg siRNA per injection per mouse), T-siPLK1-NP exhibited significantly reduced tumor burden in the lungs compared to the saline and T-siSCR-NP groups (Fig. 4C). This was also reflected in the constant body weight of the animals treated with T-siPLK1-NP, while those treated with saline and T-siSCR-NP experienced weight loss likely due to advanced cancer metastases (Fig. 4D). At 2 days after the last dose, the study was concluded and the organs from each mouse were imaged *ex vivo* with IVIS (Supplementary Fig. S5C). Tumor incidence rates (organs with positive IVIS signals relative to the respective organs of normal mice) as well as tumor burden (photon flux relative to the respective organs of normal mice) were tabulated in Table 1. Tumors were detected in fewer organs with the T-siSCR-NP treatment (vs. untreat) and in fewest organs with T-siPLK1-NP treatment (Table 1). H&E-stained and immunofluorescent tissue images are shown in Supplementary Fig. S6. The data suggest a reduction in cancer metastatic potential to distant sites by the T-NP (with just siSCR), which is consistent with our in vitro data in Fig. 3, while siPLK1 on the nanoparticle inhibited cancer growth.

T-siPLK1-NP impedes tumor proliferation and promotes cancer apoptosis in the lungs

In addition to metastasis incidence rate and tumor burden, we carefully characterized the cancer in lungs of mice to confirm the treatment efficacy of T-siPLK1-NP. T-siPLK1-NP treatment significantly reduced the tumor lesion area (by H&E, which was confirmed by human vimentin staining) in lungs by 91% and 89% compared to the saline and T-siSCR-NP groups, respectively (Fig. 4E). The extent of human cancer in mouse lungs was also

quantified by the relative levels of human HPRT (*h*HPRT) mRNA to mouse HPRT mRNA (*m*HPRT). In agreement with the histological data, T-siPLK1-NP decreased *h*HPRT mRNA by 84% and 79% compared to the saline and T-siSCR-NP groups, respectively (Fig. 4F). Lastly, we confirmed that the therapeutic effect was the direct result of RNAi by assessing the level of PLK1 knockdown. T-siPLK1-NP treatment effectively depleted PLK1 gene expression by 84% and 81% compared to the saline and T-siSCR-NP groups, respectively (Fig. 4G). Immunostaining for Ki-67 and cleaved-caspase 3 also confirmed that T-siPLK-NP caused a significant reduction in overall proliferation (Fig. 4H) and increase in apoptosis (Fig. 4I). Taken together, these experiments showed that our nanoparticle effectively delivered siPLK1 to metastatic tumors upon systemic delivery, which resulted in reduced tumor growth and increased cancer death.

Depletion of PLK1 by T-siPLK1-NP inhibits lung metastasis and prolongs overall survival in long-term *in vivo* study

To investigate the long-term therapeutic effect of T-siPLK1-NP treatment, we conducted a long-term study in which mice received the same dosing schedule as the short-term study but extended the study to 2 months (see dash lines in Fig. 5A for injection days). Tumor burden was monitored up to day 32 post 1st treatment where >80% of mice were still alive. As expected, T-siPLK1-NP significantly reduced tumor burden in the lungs as measured by 100-fold less of bioluminescence signal vs. saline (Fig. 5A). Also, the T-siPLK1-NP treatment significantly prolonged the overall survival (Fig. 5B). In addition, upon sacrifice/death, we observed large axillary lymph node tumors (>1200 mm^3) in multiple mice from the saline and T-siSCR-NP groups (4 out of 8 in each group), whereas only 1 out of 8 mice in the T-siPLK1-NP group exhibited large lymph node tumors. T-siPLK1-NP treatment also yielded smaller lung lesions as compared to saline and T-siSCR-NP groups (Supplementary Fig. S7), which agrees with the results from the short-term study. In summary, treatment with T-siPLK1-NP elicits anti-metastatic activity and extends overall survival in mice, which provides a novel potential therapeutic option for metastatic breast cancer disease.

Discussion

Herein, we have shown for the first time that mesoporous silica nanoparticles (MSNP) can scavenge intracellular ROS, modulate NOX4 activity, and in turn inhibit cellular invasion and migration in breast cancer cells *in vitro*. The ROS scavenging ability of MSNP is thought to be contributed by its extremely large surface area with protonated sites (from the acid reflux to remove surfactants during the MSNP synthesis). This intrinsic property of mesoporous silica nanoparticle hence further promotes its use as a therapeutic delivery platform for cancer treatment. We believe this finding is impactful as it may inspire new platforms that are not only passive carriers but also therapeutics. For human use, MSNP is more promising than other antioxidant nanoparticles (such as fullerene, platinum, cerium oxide) because MSNP is more benign and soluble at physiological pH to silicic acid for kidney clearance (30). Silicon (Si) is also the most abundant trace element in the human body after iron and zinc (31).

High-MW PEI (>20-kDa) is needed to form a dense siRNA-polyplex for good transfection efficacy (e.g., jetPEI™, which underwent clinical trials (32)). We used smaller PEI 10-kDa) for less toxicity while enhancing efficacy by cross-linking the PEI layer. The cross-linking increased the buffering capacity (4) leading to greater endosomal escape of siRNA based on proton sponge effect principle (33). siRNA released from the PEI layer by displacement of heparan sulfate (similar size and charge with siRNA) and by reducing of the cross-linker by glutathione. The detailed mechanism will be reported in due course.

This nanotherapeutic (siRNA-nanoparticle) was effective in treating metastatic breast cancer by simultaneously reducing metastasis potential of cancer through the intrinsic antioxidant property of the nanoparticle and delivering siPLK1 to metastatic tumors to promote apoptosis in those tumors through PLK1 gene silencing mechanism. As previously discussed, PLK1 inhibitors have shown to impart adverse effects and siPLK1 on lipid nanoparticles without a targeting agent only provided a narrow therapeutic window in clinical trials. The sequence specificity of siPLK1 combined with the tumor targeting ability of our nanoparticle platform will potentially improve both efficacy and safety for treating metastatic breast cancer. The unique antioxidant features and the versatility of our nanoparticles will potentially be beneficial in the treatment of not only cancer but also other fibrotic diseases.

Supplementary Material

Refer to Web version on PubMed Central for supplementary material.

Acknowledgments

Financial Support: This work was funded by NIH/NCI contract# HHSN261201300078C (W. Yantasee, W. Ngamcherdtrakul, D.J. Castro, J. W. Gray), the Prospect Creek Foundation (J. W. Gray, W. Yantasee), and OHSU's VPR fund (W. Yantasee).

The authors are grateful to Prof. Sara Courtneidge of OHSU for independent reviewing of the data in this paper, and to Prof. Robert Kerbel at University of Toronto and Dr. Giulio Francia at University of Texas at El Paso for generous gift of LM2-4luc+/H2N breast cancer cell line. We thank Dr. Shinji Iizuka for sharing his expertise on the gel degradation/invadopodia assays. We thank Tiera Liby in Gray's Lab for TNBC cell lines. We also thank the Transgenic Core of Oregon Health and Science University (Dr. Lev Fedorov) for SCID hairless SHO™ mouse breeding.

References

1. Ferlay, J., Soerjomataram, I., Ervik, M., Dikshit, R., Eser, S., Mathers, C., et al. GLOBOCAN 2012 v1.1, Cancer Incidence and Mortality Worldwide: IARC Cancer Base No. 11. Lyon, France: International Agency for Research on Cancer; 2014.
2. NIH National Cancer Institute. 2016 Surveillance, Epidimiology, and End Results Program. SEER Stat Fact Sheets: Female Breast Cancer.
3. Ngamcherdtrakul W, Castro DJ, Gu S, Morry J, Reda M, Gray JW, et al. Current development of targeted oligonucleotide-based cancer therapies: Perspective on HER2-positive breast cancer treatment. Cancer treatment reviews. 2016; 45:19–29. [PubMed: 26930249]
4. Ngamcherdtrakul W, Morry J, Gu S, Castro DJ, Goodyear SM, Sangvanich T, et al. Cationic Polymer Modified Mesoporous Silica Nanoparticles for Targeted siRNA Delivery to HER2+ Breast Cancer. Advanced Functional Materials. 2015; 25:2646–2659. [PubMed: 26097445]
5. Winkles JA, Alberts GF. Differential regulation of polo-like kinase 1, 2, 3, and 4 gene expression in mammalian cells and tissues. Oncogene. 2005; 24:260–266. [PubMed: 15640841]

6. Degenhardt Y, Lampkin T. Targeting Polo-like Kinase in Cancer Therapy. Clinical Cancer Research. 2010; 16:384–389. [PubMed: 20068088]
7. Maire V, Nemati F, Richardson M, Vincent-Salomon A, Tesson B, Rigaill G, et al. Polo-like kinase 1: a potential therapeutic option in combination with conventional chemotherapy for the management of patients with triple-negative breast cancer. Cancer research. 2013; 73:813–823. [PubMed: 23144294]
8. Hu K, Law JH, Fotovati A, Dunn SE. Small interfering RNA library screen identified polo-like kinase-1 (PLK1) as a potential therapeutic target for breast cancer that uniquely eliminates tumor-initiating cells. Breast cancer research : BCR. 2012; 14:R22. [PubMed: 22309939]
9. Frost A, Mross K, Steinbild S, Hedbom S, Unger C, Kaiser R, et al. Phase i study of the Plk1 inhibitor BI 2536 administered intravenously on three consecutive days in advanced solid tumours. Curr Oncol. 2012; 19:e28–e35. [PubMed: 22328845]
10. Weiß L, Efferth T. Polo-like kinase 1 as target for cancer therapy. Experimental Hematology & Oncology. 2012; 1:38. [PubMed: 23227884]
11. Raab M, Kappel S, Kramer A, Sanhaji M, Matthess Y, Kurunci-Csacsko E, et al. Toxicity modelling of Plk1-targeted therapies in genetically engineered mice and cultured primary mammalian cells. Nat Commun. 2011; 2:395. [PubMed: 21772266]
12. Arbutus. Arbutus Reports Topline Results from TKM-PLK1 HCC Clinical Trial. VANCOUVER, B.C. and DOYLESTOWN, P.A.: GLOBE NEWSWIRE; 2016.
13. Ramanathan, RK., Hamburg, SI., Borad, MJ., Seetharam, M., Kundranda, MN., Lee, P., et al. A phase I dose escalation study of TKM-080301, a RNAi therapeutic directed against PLK1, in patients with advanced solid tumors. Washington, DC: 2013.
14. Liou G-Y, Storz P. Reactive oxygen species in cancer. Free radical research. 2010; 44:479–496. [PubMed: 20370557]
15. Diaz B, Shani G, Pass I, Anderson D, Quintavalle M, Courtneidge SA. Tks5-dependent, Nox-mediated Generation of Reactive Oxygen Species is Necessary for Invadopodia Formation. Science signaling. 2009; 2:ra53. [PubMed: 19755709]
16. Boudreau HE, Casterline BW, Rada B, Korzeniowska A, Leto TL. Nox4 involvement in TGF-beta and SMAD3-driven induction of the epithelial-to-mesenchymal transition and migration of breast epithelial cells. Free radical biology & medicine. 2012; 53:1489–1499. [PubMed: 22728268]
17. Zhang C, Lan T, Hou J, Li J, Fang R, Yang Z, et al. NOX4 promotes non-small cell lung cancer cell proliferation and metastasis through positive feedback regulation of PI3K/Akt signaling. Oncotarget. 2014; 5:4392–4405. [PubMed: 24946933]
18. Hong S-Y, Gil H-W, Yang J-O, Lee E-Y, Kim H-K, Kim S-H, et al. Effect of High-Dose Intravenous N-acetylcysteine on the Concentration of Plasma Sulfur-Containing Amino Acids. The Korean Journal of Internal Medicine. 2005; 20:217–223. [PubMed: 16295780]
19. Cifuentes-Pagano E, Meijles DN, Pagano PJ. The quest for selective nox inhibitors and therapeutics: challenges, triumphs and pitfalls. Antioxidants & redox signaling. 2014; 20:2741–2754. [PubMed: 24070014]
20. MBCAlliance. Metastatic Breast Cancer Landscape Analysis: Research Report October 2014. New York, NY: Metastatic Breast Cancer Alliance; 2014.
21. Clogston, JD., Patri, AK. NCL Method PCC-2: Measuring Zeta Potential of Nanoparticles. Frederick, MD: Nanotechnology Characterization Laboratory; 2009.
22. Francia G, Man S, Lee C-J, Lee CR, Xu P, Mossoba ME, et al. Comparative Impact of Trastuzumab and Cyclophosphamide on HER-2–Positive Human Breast Cancer Xenografts. Clinical Cancer Research. 2009; 15:6358–6366. [PubMed: 19825954]
23. Morry J, Ngamcherdtrakul W, Gu S, Goodyear SM, Castro DJ, Reda MM, et al. Dermal delivery of HSP47 siRNA with NOX4-modulating mesoporous silica-based nanoparticles for treating fibrosis. Biomaterials. 2015; 66:41–52. [PubMed: 26196532]
24. Wang Z, Li Y, Sarkar FH. Signaling Mechanism(S) of Reactive Oxygen Species in Epithelial-Mesenchymal Transition Reminiscent of Cancer Stem Cells in Tumor Progression. Curr Stem Cell Res Ther. 2010; 5:74–80. [PubMed: 19951255]
25. Liang CC, Park AY, Guan JL. In vitro scratch assay: a convenient and inexpensive method for analysis of cell migration in vitro. Nat Protoc. 2007; 2:329–333. [PubMed: 17406593]

26. Le Gal K, Ibrahim MX, Wiel C, Sayin VI, Akula MK, Karlsson C, et al. Antioxidants can increase melanoma metastasis in mice. Science Translational Medicine. 2015; 7:308re8.

27. Kenny PA, Lee GY, Myers CA, Neve RM, Semeiks JR, Spellman PT, et al. The morphologies of breast cancer cell lines in three-dimensional assays correlate with their profiles of gene expression. Molecular Oncology. 2007; 1:84–96. [PubMed: 18516279]

28. Munoz R, Man S, Shaked Y, Lee CR, Wong J, Francia G, et al. Highly Efficacious Nontoxic Preclinical Treatment for Advanced Metastatic Breast Cancer Using Combination Oral UFT-Cyclophosphamide Metronomic Chemotherapy. Cancer research. 2006; 66:3386–3391. [PubMed: 16585158]

29. Milsom CC, Lee CR, Hackl C, Man S, Kerbel RS. Differential Post-Surgical Metastasis and Survival in SCID, NOD-SCID and NOD-SCID-IL-2Rγ(null) Mice with Parental and Subline Variants of Human Breast Cancer: Implications for Host Defense Mechanisms Regulating Metastasis. PLoS ONE. 2013; 8:e71270. [PubMed: 23967178]

30. Tarn D, Ashley CE, Xue M, Carnes EC, Zink JI, Brinker CJ. Mesoporous silica nanoparticle nanocarriers: biofunctionality and biocompatibility. Accounts of chemical research. 2013; 46:792–801. [PubMed: 23387478]

31. Jugdaohsingh R. SILICON AND BONE HEALTH. The journal of nutrition, health & aging. 2007; 11:99–110.

32. Sidi AA, Ohana P, Benjamin S, Shalev M, Ransom JH, Lamm D, et al. Phase I/II Marker Lesion Study of Intravesical BC-819 DNA Plasmid in H19 Over Expressing Superficial Bladder Cancer Refractory to Bacillus Calmette-Guerin. The Journal of Urology. 2008; 180:2379–2383. [PubMed: 18950807]

33. Behr J-P. The Proton Sponge: a Trick to Enter Cells the Viruses Did Not Exploit. CHIMIA International Journal for Chemistry. 1997; 51:34–36.

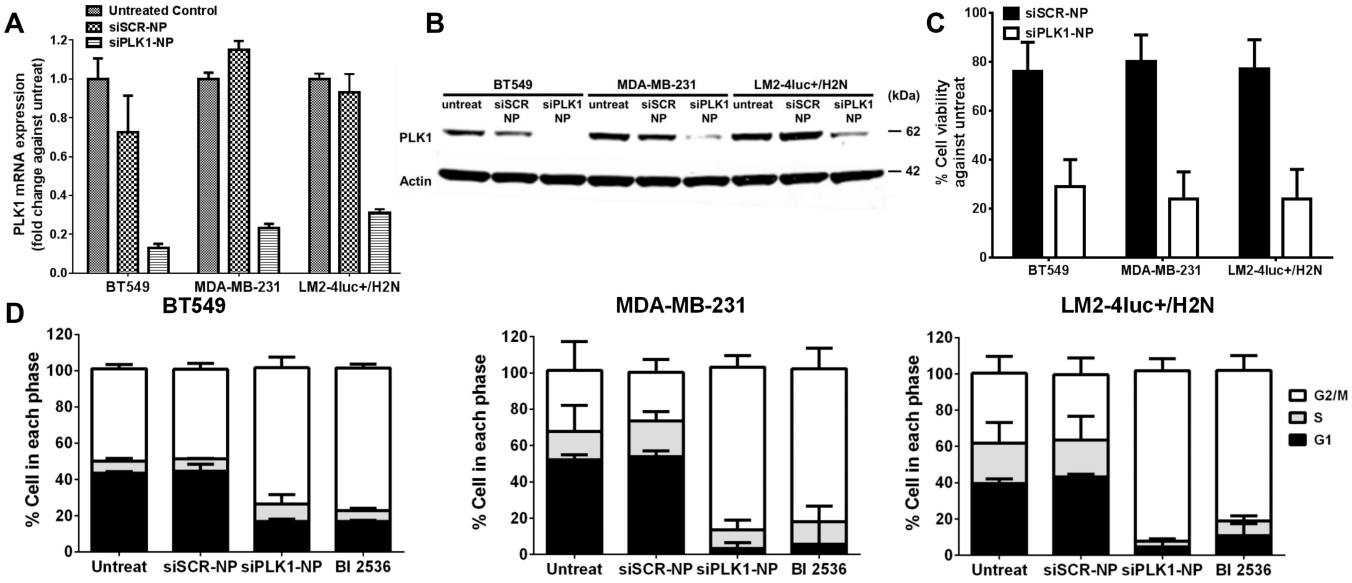

Figure 1.

Effective knockdown of PLK1 with siPLK1-NP leads to G2/M cell cycle arrest and reduced viability of three TNBC cell lines (BT549, MDA-MB-231, and LM2-4luc+/H2N). (A) Expression levels of PLK1 mRNA after treated with either siSCR- or siPLK1-NP for 24 h, as measured by qPCR, and normalized to GAPDH expression. (B) Protein expression of PLK1 after 48 h, as assessed by western blot with Actin as the loading control. (C) Cell viability after 72 h. (D) Cell cycle analysis after 24 h treatment with siSCR-, siPLK1-NP, or 10 nM of BI2536. All with siRNA dose of 50 nM. All data are presented as mean ± SD from 3 independent experiments.

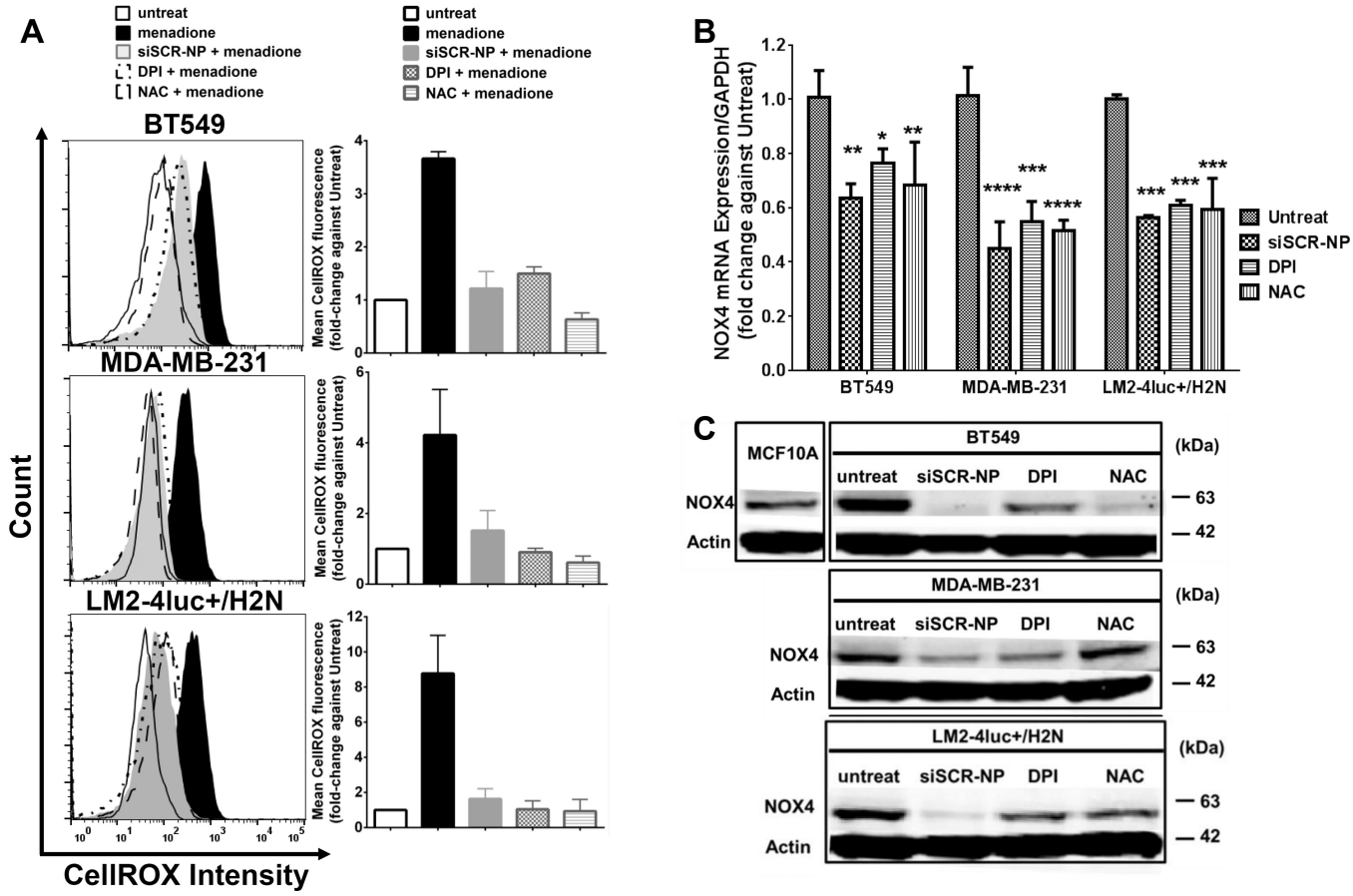

Figure 2.

NP shows antioxidant activity and NOX4 reduction in three TNBC cell lines (BT549, MDA-MB-231, and LM2-4luc+/H2N). (A) ROS levels of the cells after 24 h treatment with siSCR-NP (50 nM), DPI (5 μM), or NAC (20 mM), followed by 1 h treatment with 100 μM of menadione, assessed by CellROX flow cytometry. (B) Expression levels of NOX4 mRNA at 24 h and (C) NOX4 protein at 72 h of the three cell lines after receiving similar treatments with (A) for 24 h but without menadione. All mRNA data were measured by qPCR and normalized to GAPDH expression. Data are presented as mean ± SD from 3 independent experiments. *P<0.05, **P<0.01, ***P<0.001, ****P<0.0001 vs. untreat.

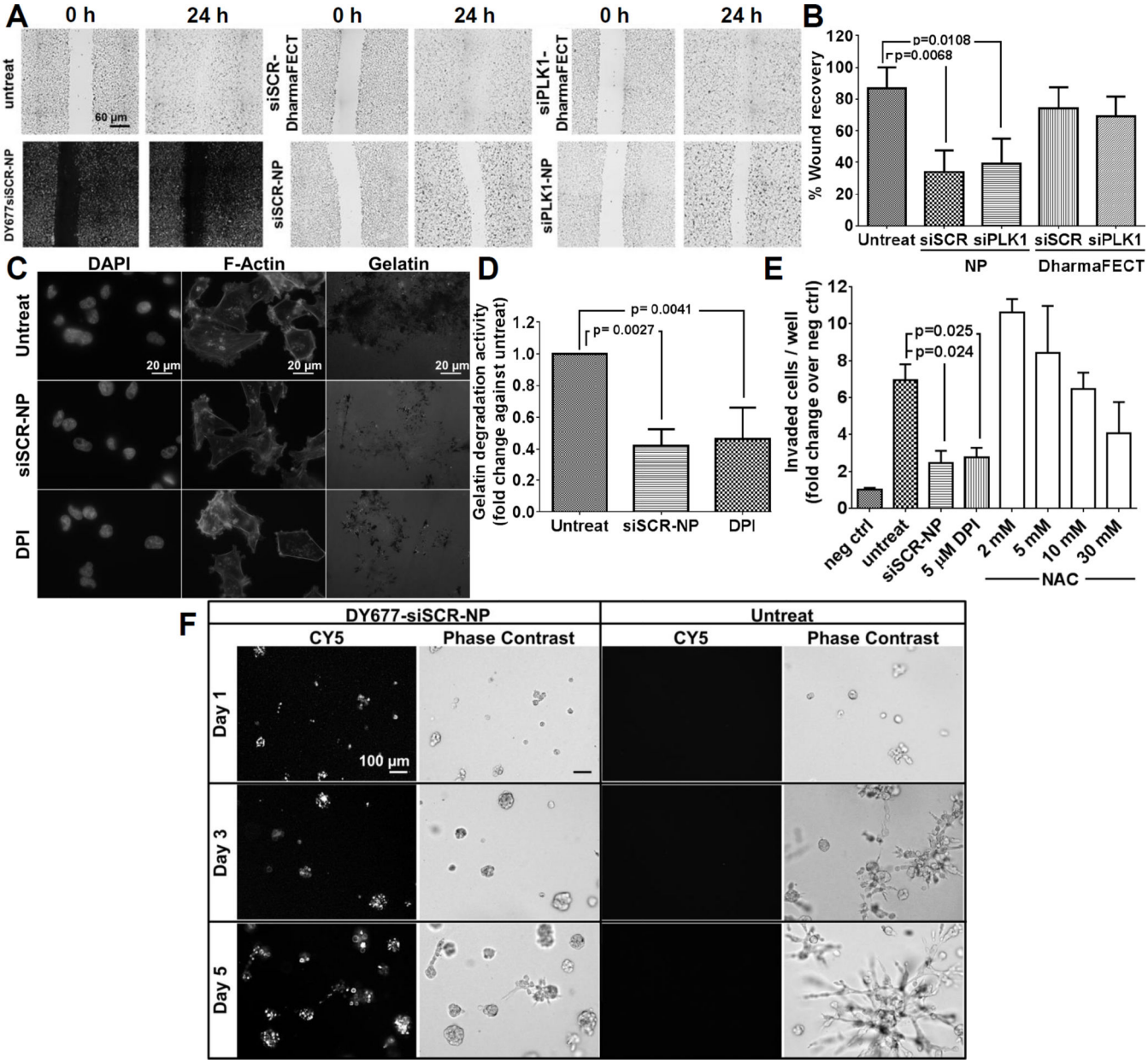

Figure 3.

NP treatment impedes cellular migration and reduces cellular invasiveness of LM2-4luc +/H2N cell line. (A) Representative images of in vitro scratch assay with siSCR or siPLK1 on NP, or on DharmaFECT (all with 50 nM as siRNA). Cells were treated for 24 h prior to wound scratch and images were taken at 0 h and 24 h post-scratch. (B) The percent wound recovery area from (A) using ImageJ. Data are presented as mean ± SD from 3 independent experiments (n=8-10 images/well, duplicate wells per experiment). (C) Representative images from gelatin degradation assay. Cells were pre-treated with 50 nM siSCR-NP or 5 µM DPI prior to seeding on the FITC-gelatin coated coverslips for 24 h. Cells were stained for F-actin and nuclei. (D) The percentage of gelatin degradation per total number of cells in (C) by ImageJ. Data are presented as mean ± SD from 3 independent experiments (n = 5

images/well, >50 cells/field, duplicate wells per experiment). (E) Invasion of LM2-4luc +/H2N cells after 48 h treatment with 50 nM siSCR-NP, 5 μM DPI, or 2–30 mM NAC through Matrigel-coated Boyden chambers, normalized by negative controls (number of cells invaded through chambers with no serum added). Data are represented as mean ± SD from two independent experiments performed in duplicates. (F) Representative images of LM2-4luc+/H2N cells pretreated with 50 nM DY677siSCR-NP prior to seeding in 3D matrigel culture vs. untreat and imaged on day 1, 3, and 5 post-seeding.

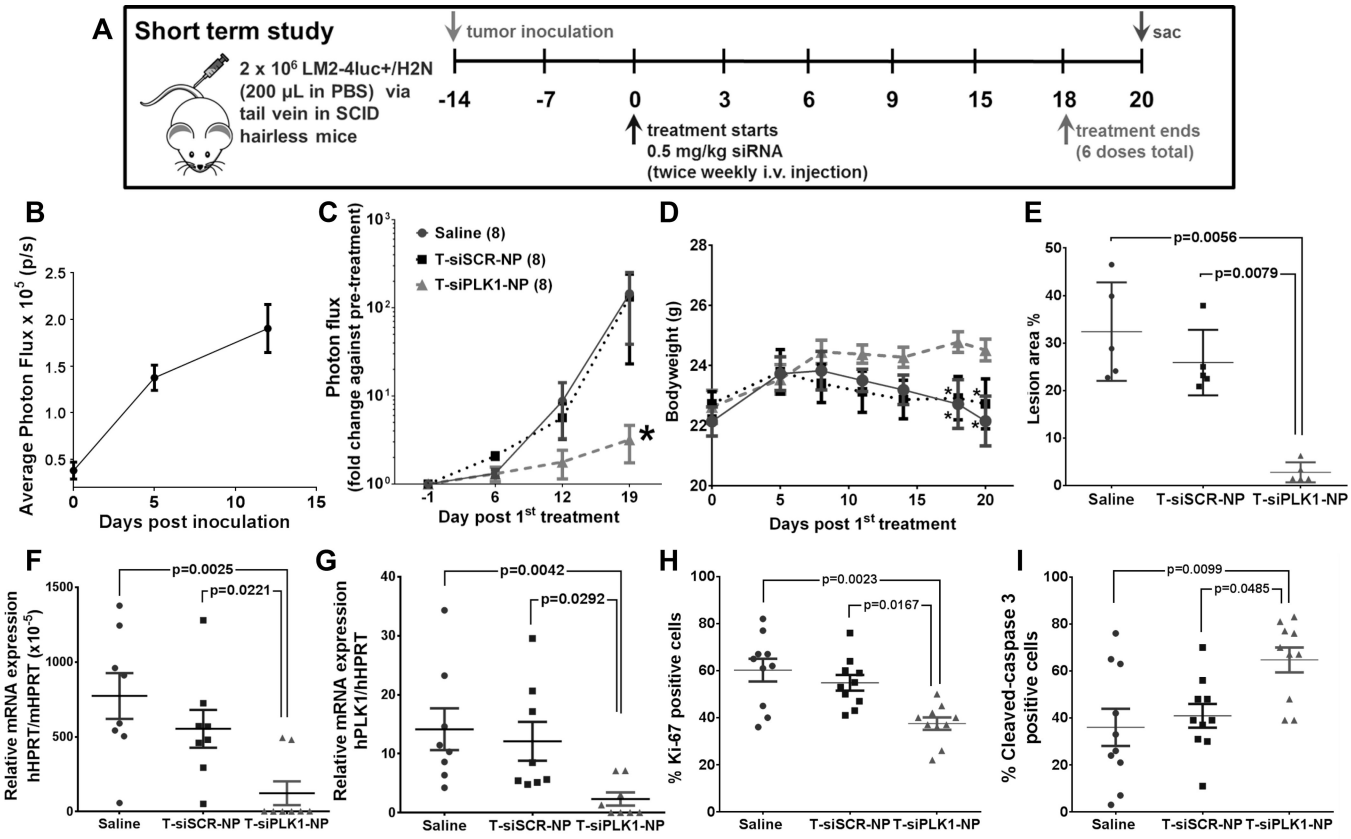

Figure 4.

Effects of T-siPLK1-NP treatment in the *in vivo* experimental metastasis model. (A) Schematic representation of the study design for the short-term *in vivo* study. (B) Quantification of lung photon flux (by weekly IVIS) showing cancer being established in lungs post inoculation. (C) The lung photon flux normalized to pre-treatment flux from each individual mouse in the same treatment groups. (D) Average body weight of mice in each treatment groups during the study period. Tumor burden in lungs as quantified by (E) percent tumor lesion area per total lung area (see Supplementary Fig. S6A for images) and by (F) qPCR analysis of human HPRT (*h*HPRT) mRNA relative to mouse HPRT (*m*HPRT) in mouse lungs. (G) Knock down of PLK1 mRNA, quantified by *h*PLK1 mRNA expression in the lung tissues relative to *h*HPRT mRNA. *h* stands for human. (H) Percent Ki-67 positive cells in the lung nodes (see Supplementary Fig. S6B for images). (F) Percent cleaved-caspase 3 (CC3) positive cells in the lung nodes (see Supplementary Fig. S6C for images). All data are represented as average ± SEM (n = 24 for (B) and n = 8/group for (C&D). Each dot in (E–G) represents value from one mouse, and in (H&I) represents one tumor node in the lungs of mice (n=2 nodes/mouse, 5 mice/group). Data are presented as mean ± SEM (n=24 for (B) and n=8/group for (C&D)). *p<0.05 from Two-way ANOVA followed by Dunnett's multiple comparison tests for (C&D). P values as indicated on (E-I) from Kruskal-Wallis test.

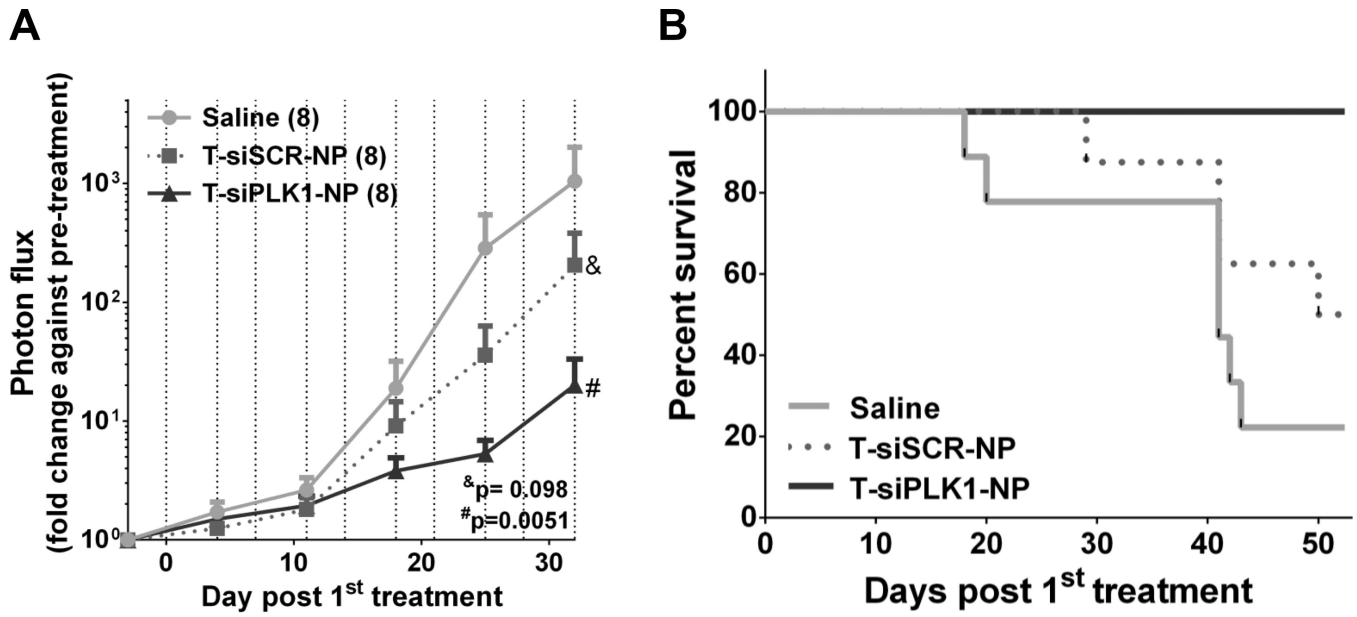

Figure 5.

T-siPLK1-NP treatment improves overall survival of LM2-4luc+/H2N experimental metastasis mice. (A) Quantification of lung photon flux normalized to pre-treatment flux from each individual mouse in the treatment groups (n=8/group). Data are presented as mean ± SEM. P values as indicated on the graph from Two-way ANOVA followed by Dunnett's multiple comparison tests. Vertical dashed lines represent injection days. (B) Kaplan-Meier survival of mice (n=8/group). Data are presented as mean ± SEM. *P=0.0251 between T-siPLK1-NP *vs.* Saline by Mantel-Cox Log rank test. H&E and DAPI/Vimentin Stains of lung samples can be found in Supplementary Fig. S7.

Table 1

Incidence rate of LM2-4luc+/H2N metastasis in various organs of mice receiving a total of 6 doses of either T-siPLK1-NP or T-siSCR-NP, as quantified by *ex vivo* IVIS imaging as shown in Supplementary Fig. S5(C). The tumor signal in each organ is reported as fold-change over the signal from the same organ of normal mice (n=4 for normal mice, n=8 mice/treatment group). Dose and schedule as shown in Fig. 4(A).

Group	Parameter	Brain	Lung	Liver	Spleen	Kidney	Lymph nodes	Spine	Total tumor signal	Ratio over saline
Saline	Incidence rate	2/8	8/8	2/8	1/8	1/8	5/8	4/8		
	Tumor signal	288	405	73	16	12	240	1717	2749	1.00
T-siSCR-NP	Incidence rate	1/8	7/8	-	-	-	4/8	4/8		
	Tumor signal	139	443	-	-	-	131	1322	2036	0.74
T-siPLK1-NP	Incidence rate	-	4/8	-	-	-	1/8	3/8		
	Tumor signal	-	26	-	-	-	3	939	968	0.35